Title

The bias of a two-dimensional view: comparing two-dimensional and three-dimensional mesophyll surface area estimates using noninvasive imaging

Journal

New Phytologist, 215(4)

ISSN

0028-646X

Authors

Théroux-Rancourt, Guillaume
Earles, J Mason
Gilbert, Matthew E
et al.

Publication Date

2017-09-01

DOI

10.1111/nph.14687

Peer reviewed

The bias of a 2D view: Comparing 2D and 3D mesophyll surface area estimates using non-invasive imaging

Guillaume Théroux-Rancourt[1]*, J. Mason Earles[2]*, Matthew E. Gilbert[1], Maciej A. Zwieniecki[1], C. Kevin Boyce[3], Andrew J. McElrone[4,5], and Craig R. Brodersen[2]

[1]Department of Plant Sciences, University of California Davis, Davis, CA, 95616
[2]School of Forestry & Environmental Studies, Yale University, New Haven, CT 06511
[3]Department of Geological Sciences, Stanford University, Stanford, CA 94305
[4]USDA-Agricultural Research Service, Davis, CA 95616
[5]Deparment of Viticulture and Enology, University of California, Davis, CA 95616
*: Equal contributions
Corresponding author: G. Théroux-Rancourt (gtrancourt@ucdavis.edu)

Summary

- The surface area of the leaf mesophyll exposed to intercellular airspace per leaf area (S_m) is closely associated with CO_2 diffusion and photosynthetic rates. S_m is typically estimated from two-dimensional (2D) leaf sections and corrected for the three-dimensional (3D) geometry of mesophyll cells, leading to potential differences between the estimated and real cell surface area.
- Here, we examined how existing 2D methods used for estimating S_m compare to 3D values obtained from high-resolution X-ray computed tomography (microCT) for 23 species, with broad phylogenetic and anatomical coverage.
- Relative to 3D S_m values, uncorrected 2D S_m estimates were 15 to 30% lower on average. Two of the four 2D S_m methods typically fell within 10% of 3D values. For most species, only one slice was needed to accurately estimate S_m within 10% of the leaf-level 3D median. However, leaves with high vein density and diverged veins (e.g. eudicots) often required multiple sections.
- These results provide the first comparison of the accuracy of 2D methods in estimating the complex 3D geometry of internal leaf surfaces. Because microCT is

not readily available, we provide guidance for using standard light microscopy techniques, as well as recommend standardization of reporting S_m values.

Keywords (5 to 8): leaf functional traits; leaf anatomy; biodiversity; CAM plants; high resolution X-ray computed tomography;

Introduction

Leaf photosynthetic function is directly linked to tissue-level anatomy which can grossly be categorized into vascular, mesophyll, and epidermal cell types. Chloroplasts predominantly inhabit mesophyll cells in the majority of higher plants and require access to sufficiently high [CO_2] to maximize net assimilation. Consequently, most terrestrial plants have evolved leaf features to facilitate intercellular CO_2 diffusion, such as amphistomatal leaves (e.g. Parkhurst & Mott, 1990) and large airspaces to facilitate lateral diffusion (Pieruschka *et al.*, 2006; Morison *et al.*, 2007). Moreover, chloroplasts are typically positioned within mesophyll cells immediately adjacent to the intercellular airspace (IAS) to minimize the liquid CO_2 diffusion path length (e.g. Evans *et al.*, 2009; Tholen & Zhu, 2011). For these reasons, the surface area of mesophyll cells per leaf area (S_m) is positively related to CO_2 diffusion and maximum leaf photosynthetic capacity (A_{max}; Nobel, 1977).

Given its underlying relationship with CO_2 assimilation, S_m is a functionally important trait to measure when comparing genotypes and phenotypes (e.g. Tholen *et al.*, 2008; Giuliani *et al.*, 2013) and when comparing growth responses to environmental factors. As one example, leaf light environment is closely associated with changes in S_m. For a given species, exposure to high light levels during development tends to result in thicker leaves with a greater proportion of palisade cells, resulting in a greater S_m with higher photosynthetic capacity (e.g. Nobel, 1976; Terashima *et al.*, 2001). As another example, plant species with a greater S_m tend toward higher A_{max} (Nobel, 1977; Longstreth *et al.*, 1980; Tosens *et al.*, 2012; Chatelet *et al.*, 2013), although other anatomical traits such as cell wall thickness (e.g. Tosens *et al.*, 2016) and the coverage of mesophyll cell surface by chloroplasts (S_c, surface of chloroplast exposed to the IAS; e.g. (Tholen *et al.*, 2008)) act to decrease mesophyll conductance to CO_2 (g_m). These, among other studies, have resulted in S_m being an anatomical trait commonly measured in plant ecophysiology.

Numerous methods have been developed for estimating mesophyll surface area, all of which are derived from two-dimensional (2D) leaf sections and optical or transmission electron microscopy. Specifically, we have found nine methods in the plant biology literature: Turrell (1936), Nobel (Nobel *et al.*, 1975; Nobel, 1976), Chabot and Chabot (Chabot & Chabot, 1977; Jurik *et al.*, 1982), Thain (1983; revisited by Evans *et al.*,

1994), Parkhurst (1982), Kubínová (e.g. Kubínová, 1994), James *et al.* (1999), Ivanova and P'yankov (2002), and Sack *et al.* (Chatelet *et al.*, 2013; Sack *et al.*, 2013). Some of these methods assume that all the cell's surface is exposed to the IAS (Nobel *et al.*, 1975; Sack *et al.*, 2013), which is not assumed by the bulk of the other methods. Another group of methods rely on stereological measurements, where assumptions on cell shape are made to infer 3D areas from 2D cross-sections (Chabot & Chabot, 1977; Parkhurst, 1982; Kubínová, 1994; Ivanova & P'yankov, 2002); these methods are more robust for randomly distributed structures and, as a result, such methods can be difficult to apply given the anisotropy often observed for leaves (Ivanova & P'yankov, 2002). Yet, estimates of S_m from 2D cross sections, regardless of the method, are necessarily approximations of the true 3D geometry of the internal leaf surfaces. To date, these methods have not been validated because of the difficulty in obtaining surface area measurements of the complexity of cellular shape and arrangement within the leaf. Efforts to improve crop performance may ultimately focus on exactly these traits (Zhu *et al.*, 2010; Evans, 2013), and without knowledge of the inherent flaws or inaccuracies related to traditional 2D methods, it will be difficult to make meaningful progress in increasing S_m if we don't know if we can accurately measure it.

Here, we compare four of the most common methods for estimating S_m from 2D leaf sections to 3D values obtained from non-invasive high resolution X-ray micro-computed tomography imaging (microCT) for leaves from 23 species that cover a broad phylogenetic and anatomical spectrum. Importantly, the differential absorption of X-ray energy by water and air allows for segmentation and quantification of intercellular airspace and mesophyll cell surface area. Further, X-ray microCT is capable of generating hundreds to thousands of leaf cross-sections with sub-micrometer thickness, which generates the necessary data to compare both 3D estimates of IAS properties, as well as established 2D methods using the same dataset. Thus, we provide recommendations regarding the estimation of S_m using both 2D and 3D techniques, which should provide a basis for comparing values obtained in previous studies and set a standard for future efforts.

Previous methods for estimating S_m

In this study, we have focused on four contrasting methods that estimate mesophyll surface area from leaf sections (a detailed review is presented in the Supplementary Information):

I) Turrell (1936) provided the earliest method to estimate S_m, and this was a method used in early landmark papers such as El-Sharkawy and Hesketh (1965). It uses paradermal slices from each cell layer and a cross section to scale 2D sections to 3D, making basic assumptions about cell distribution in each layer, it uses no correction factors but necessitates a higher number of slices to estimate S_m.

II) Thain (1983), on the other hand, provided an easy method to apply a curvature correction based on cell geometry, and this method was promoted by Evans et al. (1994), but still preferably necessitates a combination of cross and paradermal sections to achieve the best results. It is to date the most used method in the literature (32 of 51 analyzed papers).

III) James, Smith and Vogelmann (1999) presented a method using only a single section, an oblique-paradermal section, and this method was used by Slaton and Smith (2002) to compare the leaf anatomy of 56 species from 21 families, but hasn't been adopted since to our knowledge.

IV) Sack et al. (2013) present a method that allows for quantification of cellular traits based upon idealized cell shapes, while making the assumption that all mesophyll surface is exposed to the IAS.

Materials and Methods

Comparing 2D and 3D estimates

Plant material

Species were selected to represent a diversity of plant groups, leaf structure, and palisade tissue fraction (Table 1). A small group of Bromeliaceae was investigated to cover both C3 and CAM leaf types, and this group was measured using both microCT and light microscopy (see section 'Comparing embedded material to 3D data' below). Plants were grown under various conditions, which represents the usual diversity found in the literature (see Supplementary Table S1 for species details). Leaves or plant samples were

collected, their petiole/stem was wrapped in wet paper towels and immediately put in plastic bags. They were transported and scanned at the microCT facility within 36 h.

3D method: Segmentation and classification of airspace, mesophyll tissue, and veins from microCT scans of leaves.

Leaf samples were brought to the Advanced Light Source (ALS) at Lawrence Berkeley National Laboratory (LBNL) to be scanned at the microCT beamline number 8.3.2. The following steps were used to segment and classify the airspace, mesophyll tissue, and veins and are represented in Figure 1 with matching step number. The analysis allowed the scan data to be converted to a binary image of the airspace and used freely available software.

1. Sample preparation: Before each scan and up to a maximum of 30 min before scanning, one sample was excised from the leaf in a fully developed region parallel to a major vein or first order vein. Samples were ~1.5 to 2 mm wide and ~20 mm long. Samples were immediately enclosed between two pieces of Kapton (polyimide) tape to prevent desiccation while allowing high X-ray transmittance. A small portion of the sample was then inserted vertically and centered in a pipette tip. The sample in the pipette tip was brought to the microCT stage and inserted into the sample holder and centered in the X-ray beam.
2. microCT scanning: Leaf tissue was scanned using the continuous tomography mode capturing 1025 projection images at an X-ray energy of 21-25 keV. Scans were performed using either the 5x or 10x magnification, yielding final voxel resolution of 1.28 and 0.64 µm, respectively. A sample was scanned in approximately 15 minutes.
3. Reconstruction: Reconstruction was carried out using TomoPy, a Python-based framework for the reconstruction of tomographic data (Gürsoy *et al.*, 2014). Each raw dataset was reconstructed using both Gridrec (Dowd *et al.*, 1999) and phase retrieval reconstruction (Davis *et al.*, 1995). Both methods were complementary: Gridrec performed better when isolating smaller pores and material boundaries, but was not able to isolate larger voids, which were better isolated on the phase retrieval images. For each reconstruction, images stacks were rotated so that the

leaf was oriented in a cross section view and the epidermises were parallel to the image stacks' top and bottom borders, and such that their position was similar from the front until the end of the stack. When possible, veins were aligned so that they were in the same position from the front until the end of the stack. Stacks were cropped between two major veins (from middle to middle) or by removing the cut edges of the leaf sample, which were usually slightly dehydrated, so that the leaf sample filled the image from left to right. Greyscale bit depth was decreased from 32-bits to 8-bits. Final stack length was between 200 up to 2000 8-bit greyscale images. Image manipulation was applied equally among scans and done using ImageJ software (Schneider *et al.*, 2012).

4. Airspace segmentation and classification: For Gridrec and phase retrieval reconstructions, the airspace was segmented by subjectively visually defining a range of pixel values between a minimum and maximum value (i.e. threshold) such that the most airspace was accurately classified while minimizing false classification (i.e. non-airspace pixels). This resulted in a binary image stack that defined the presence or absence of airspace.
5. Combining classified images from both reconstruction methods and classifying other leaf features: Binary image stacks from both reconstructions were added together using the *Image Calculator* function in ImageJ. To get proper estimates of the IAS features, the mesophyll boundary was manually drawn out as regions of interest (ROIs) for slices where significant changes occurred, and ROIs for in-between slices were interpolated using the *Interpolate ROIs* function. The boundaries of all veins (and fibers if present) were drawn out in the same manner. We removed the vein to avoid including it as part of the total mesophyll volume and to avoid falsely classifying embolized vessels as IAS. To produce the final stack prior to analysis, the outside of the mesophyll and veins were classified with unique pixel values. We refer to this stack as 'composite stack' (stack with cells, airspace, veins, and other mesophyll), as opposed to 'binary stack' (airspace and non-airspace).

3D method: Measuring S_m and other IAS features from the image stack

To extract the IAS features and measure S_m, the composite stack was prepared by selecting only the airspace using the *Threshold* function in ImageJ. With this binary stack, airspace features were measured using BoneJ, an ImageJ plugin originally developed to analyze bone geometry and shape (Doube *et al.*, 2010 all following functions are taken from this plugin). Airspace volume and total volume of the sample were measured from voxel counts using the *Volume fraction* function. Airspace surface was measured using *Particle Analyzer* function. Potential noise in the stack was removed by analyzing any 3D particle, i.e. a group of connected voxels, larger than 3 voxels (3 × resolution^3 (μm^3)). Particles were analyzed using resampling rates of one and two. A resampling rate of one, the lowest possible value, results in a surface mesh with smaller triangles, and thus finer features are extracted. A resampling rate of two results in a smoother mesh with fewer triangles. The surface area of all the particles extracted by Particle Analyzer were summed up and used as the total mesophyll area exposed to the IAS (A_{mes}, μm^2). Mesophyll volume (V_{mes}, μm^3) was computed from the total volume of the sample minus the vein volume. Leaf sample area (LA, μm^2) was defined as the image width multiplied by stack depth. S_m was then computed as:

$$S_{m,3D} = A_{mes} / LA \quad \text{(eqn. 1)}$$

2D methods: Estimating S_m using 2D methods for individual microCT slices

For Thain's curvature correction (Morris & Thain, 1983; Thain, 1983; Evans *et al.*, 1994), the average major (*a*; length) and minor (*b*; width/diameter) axes of at least 10 adjacent cells were included within a randomly placed sampling window that included both palisade and spongy mesophyll. The major and minor axis were measured from a representative cross section slice using the Gridrec reconstructed stack (Figure 2). Curvature correction (*F*) was computed for each mesophyll tissue from the *b*/*a* ratio, and the leaf-averaged *F* was computed as (Evans *et al.*, 1994):

$$F_{leaf} = F_{sp} \times f_{sp} + F_{pal} \times f_{pal} \quad \text{(eqn. 1)}$$

where f_{sp} and f_{pal} are the fraction of spongy and palisade mesophyll. This correction factor was applied to the raw and uncorrected S_m data ($S_{m,raw}$), which is the sum of the perimeter

of each airspace area in one single slice in cross-sectional view (P) divided by the width of the cross-section (w), such that:

$$S_{m,Thain} = (P/w) \times F_{leaf} \quad \text{(eqn. 2).}$$

Note that individual $S_{m,raw}$ (P/w) and $S_{m,Thain}$ values are available for hundreds to thousands of slices, and thus summary statistics can be computed. Unless specifically stated, the median value for the entire stack is presented.

Unlike the values above based on Thain (1983), the following methods are produced from only one set of sections. For the JSV method (James *et al.*, 1999; Slaton & Smith, 2002), a line selection was drawn on the binary stack from ad- to abaxial epidermis at an angle of ~30° in a cross sectional view, and the OPS was produced by reslicing the stack, i.e. generating a new 2D image composed of the pixel values along the line selection for each slice (*Reslice* function, without interpolation). The resulting image was binarized again (*Adjust threshold* function) because of gray-valued pixels produced with the reslice. The perimeter of the airspace was measured as above and S_m was estimated as (Slaton & Smith, 2002):

$$S_{m,JSV} = \frac{P \times t}{w_{OPS} \times L_{OPS}} \quad \text{(eqn. 3)}$$

where t is the thickness of the mesophyll, measured on the Gridrec reconstruction under a cross sectional or longitudinal view, w_{OPS} and L_{OPS} are the width (along epidermis; from ~400 to 1200 pixels) and length (from ad- to abaxial epidermis; from ~800 to 2000 pixels) of the OPS (Figure 2).

For the Turrell method (Turrell, 1936), cell dimensions were measured on a cross sectional view using the Gridrec stack and averaged over at least 10 adjacent cells in a sampling window. The cell perimeter exposed to IAS and cell areas were measured on a paradermal section of the binary stack over the entire section. The palisade cell surface area was estimated by multiplying, for each layer, the height of layer ($h_{pal,i}$) by its perimeter exposed to the IAS ($P_{pal,i}$), measured under a paradermal view. For the spongy mesophyll, the vertical length of the cells (h_{sp}) was measured at an angle not greater than 45° from the vertical (i.e. h_{sp} can be a curved line, to represent to whole exposed height of the cell). The horizontal (paradermal) length of the spongy cells were measured again at an angle

not greater than 45° from the horizontal and divided into the length exposed to the IAS (l_e) and the total length (l_t), so that the horizontal exposed area could be corrected for the actual fraction that is exposed to the IAS. The perimeter exposed to the IAS (P_{sp}) and area (A_{sp}) of the spongy mesophyll cells were measured on a representative paradermal view, and the resulting area for one layer was multiplied by the average number of spongy cell layers (n_{sp}). Turrell (1936) also accounted for the surface of the abaxial epidermis exposed to the IAS as he was interested in the evaporative surface (area of the sample under a paradermal view (A_{samp}) – A_{sp}). He then estimated S_m as:

$$S_{m,Turrell} = \frac{\sum_{i=1}^{n_{pal}} h_{pal,i}P_{pal,i} + n_{sp}\left(h_{sp}P_{sp}+2A_{sp}\frac{l_e}{l_t}\right) + \left(A_{samp}-A_{sp}\right)\frac{l_i}{w}}{A_{samp}} \quad \text{(eqn. 4)}$$

where n_{pal} is the number of palisade cells layers (all anatomical components are presented in Figure 2). Note that the numerator is composed of the palisade (1st term in eqn. 4), spongy (2nd term in eqn. 4) and abaxial epidermis (3rd term in eqn. 4) components. Since the comparison conducted here uses all the exposed surface, the abaxial epidermis term is relevant, but this term could be removed if only chlorenchymous tissue is of interest. Note that Turrell (1936) applied a correction to the abaxial epidermis term by measuring the length of the inner wall of the epidermis in the cross-sectional view (l_i) as the width of the cross section being measured (w). This might be less relevant, however, when using digital imaging where the section can be easily rotated so that $l_i \approx w$.

For the Sack et al. method (Chatelet *et al.*, 2013; Sack *et al.*, 2013), cellular dimensions are used to compute each cell's surface area and volume, which is subsequently used to estimate the number of cells per tissue. Here, spongy mesophyll cells are assumed to be spheres with a circumference equal to the cell perimeter (p_{sp}), measured on a cross section of the Gridrec stack. Palisade cells are assumed to be cylinders with hemispherical ends, and the length (h_{pal}) and diameter (d_{pal}) axes were measured on a cross-sectional view (Figure 2). The surface of mesophyll per leaf area is then computed as:

$$SA_{pal} = 2\pi\frac{d_{pal}}{2h_{pal}}, \quad V_{pal} = \pi\left(\frac{d_{pal}}{2}\right)^2\left(\frac{4}{3}\times\frac{d_{pal}}{2} + h_{pal} - d_{pal}\right)$$

279 $$SA_{sp} = 4\pi\left(\frac{p_{sp}}{2\pi}\right)^2, \;\; V_{sp} = \frac{4}{3}\pi \times \left(\frac{p_{sp}}{2\pi}\right)^3 \quad \text{(eqn. 5)}$$

280 $$S_{m,Sack} = \frac{\overline{SA}_{pal} \times t_{pal}(1-\theta_{pal})}{\bar{V}_{pal}} + \frac{\overline{SA}_{sp} \times t_{sp}(1-\theta_{sp})}{\bar{V}_{sp}}$$

281 where SA and V are the surface area and volume of one cell, and θ is the porosity of the
282 tissue (area IAS (μm^2) / mesophyll area (μm^2)).
283
284 *Identifying the minimum number of slices needed to produce a reliable S_m estimate*
285 Using the data from each individual slice (i.e. all $S_{m,raw}$ values for one leaf), we
286 estimated the number of 2D sections needed to estimate S_m within 5 or 10% of the leaf
287 level median with 95% confidence. To do so, we reordered the S_m values for each species
288 to create 10 000 random sets. The median value was then calculated for each reordered
289 set for an increasing number of slices, using only one S_m value up to 500 or the max
290 number of slices for that species, whichever is reached first. This created 10 000 median
291 values for each number of slices used to compute the median. The 5th and 95th were
292 computed, and the smallest number of slices needed to be within 5 and 10% was
293 identified. This was computed using R 3.3.3 (R Core Team, 2017).
294
295 *Comparing embedded material measured with light microscopy to 3D data*
296 Bromeliaceae leaf samples, from the same leaf scanned with microCT when
297 possible, were embedded and prepared for microscopy using methods from Bozzola &
298 Russell (1999), and Russin & Trivett (2001). Leaves were fixed in Karnovsky's fixative.
299 Tissues were rinsed with 0.1M PO_4 buffer and post-fixed for 2 h in 1% buffered osmium
300 tetroxide. Leaves were dehydrated with ascending concentrations of ethyl alcohol with
301 three changes at 100%, transitioned 1:1 with propylene oxide, and dehydrated using two
302 changes of pure propylene oxide. Infiltration began using Epon/Araldite resin in three
303 ascending concentrations with propylene oxide. Finally, three changes of resin with
304 microwave assistance were done before overnight polymerization in capsules. Semi-thin
305 sections were cut using a Leica Ultracut UCT ultramicrotome and were stained with 2%
306 Methylene Blue/Azure II before being observed at 20× magnification with an Axio Imager
307 A2 microscope (Zeiss, Oberkochen, Germany).

Structural traits, t, θ_{IAS}, P, w, and the total area of the mesophyll (A_{mes}; not including vein area), were analyzed using ImageJ software. To normalize for uneven leaf thickness between the embedded section and the microCT stack, the ratios $P/A_{mes,2D}$ (μm μm^{-2}; see also Nelson *et al.*, 2005) and $A_{mes,3D}/V_{mes,3D}$ (μm^2 μm^{-3}) were compared.

Results

The 23 species analyzed spanned a broad range of mesophyll thickness (95 to 670 μm), porosity and fraction of palisade tissue within the leaf, from the spongy-only fern *Asplenium nidus* and the CAM orchid *Oncidium ornithorhynchum*, to the palisade-only *Welwitschia mirabilis* (Table 1; see Supplementary Figure S1 for a representative cross section of each species taken from the microCT). Using the microCT data, S_m ($S_{m,3D}$) was estimated with two resampling rates. A resampling rate of one (R1) produced $S_{m,3D}$ ($S_{m,3D\text{-}R1}$) values 10 to 70% higher (average 25%) than when using a resampling rate of two (R2; $S_{m,3D\text{-}R2}$). R2 produces a smoother surface mesh by using larger triangles, and this resulted in some particles, i.e. individual airspace volumes, having zero surface points, hence no triangle captured the small size of those particles – an example of the coastline paradox (). Consequently, small diameter pores, i.e. close to the resolution limit of the image, were captured less accurately at a higher resampling rate. *Oncidium ornithorhynchum* showed the largest difference between R1 and R2, where the mesophyll consists of tightly packed spheroids with a very low porosity (0.04) and narrow air passages. Leaves with packed palisade cells of small diameter like *Gossypium* and *Prunus* also showed a large difference between R1 and R2. Further, a smaller resolution (or higher magnification) generally led to a larger difference between R1 and R2 (+27% with a magnification of 5x, or 1.28 μm pixel^{-1}, vs. +19% with a magnification of 10x, or 0.64 μm pixel^{-1}).

The $S_{m,raw}$ values, i.e. the uncorrected length of mesophyll exposed to the IAS divided by the section width, had a median value of 16% less than $S_{m,3D\text{-}R2}$ and 32% less than $S_{m,3d\text{-}R1}$ (Figure 3). Using the JSV oblique-paradermal section method produced $S_{m,2D}$ estimates with slightly less difference than with $S_{m,3D}$ values (-26% vs. R1 and -8% vs. R2; Figure 3), yet the estimates were in a broader range than $S_{m,raw}$. The Sack *et al.* (2013) method, which estimates the entire cell surface and assumes that it is completely exposed

to the IAS, produces $S_{m,Sack}$ values having a median +157% from the $S_{m,3D\text{-}R1}$, with values ranging from -52% to +552% (Table 1).

$S_{m,Thain}$ and $S_{m,Turrell}$ values were similar to each other and most closely matched the 3D values, being within a median ±10% of the 3D values, for both R1 and R2. Generally, the species that were corrected to be within 10% of $S_{m,3D\text{-}R1}$ value with the Thain method had a similar difference when comparing the estimates from the Turrell method. However, several species had better estimates with the Turrell method compared to the Thain method (e.g. *Monstera*, *Guzmania*, *Austrobaileya*; see Table 1). All leaf types performed well with both Thain's and Turrell's methods, where leaves with high porosity (e.g. *Helwingia* and *Nymphaea*) and low porosity (e.g. *Aechmea fendleri* and *Platycerium*, both CAM plants) were within 10% of the $S_{m,3D\text{-}R1}$ value. Species with a broad range of mesophyll thickness was also included within that range.

For most species (15 out of 23), one to three sections were necessary to estimate $S_{m,2D}$ within 10% of the whole leaf median, 95% of the time (Figure 4). For those species, a few more slices were needed to be within 5% of the leaf median and up to a total of 10 slices. The species which needed the highest number of slices to be within 10% of the leaf median (> 4 and up to 10) required substantially more slices to be within 5% (13 up to 35). Those high number of slices species were mainly Eudicots with diverged veins, or species with greater heterogeneity among slices (see Figure 5). However, when the slices with a high proportion of veins were removed, a common subjective practice when analyzing microscopic slices, the minimum number of slices typically decreased substantially, with for example a decrease from 8 to 2 slices for *Gossypium* (Figure 4). This narrowed the range of $S_{m,2D}$ values and removed the low valued outliers, which were mainly slices with a high proportion of veins (Figure 5). In comparison, *Myriopteris*, which needs only one slice to be within 10% of the leaf median, is very homogenous throughout the leaf sample (Figure 5).

Using embedded material from six bromeliad species, we compared the methods to estimate the surface of mesophyll. Applying a Thain (1983) correction to the total perimeter of mesophyll measured per mesophyll area measured on embedded material resulted in similar differences with the mesophyll surface area over mesophyll volume ratio measured from the microCT data (Figure 6a). Interestingly, the species that had the

largest difference between the 2D and 3D value were the thickest leaves (~400 µm), while the thinnest leaves (~100 µm) produced very similar values (Figure 6b). Species with thicker leaves resulted in up to ~40% less surface being estimated from embedded material compared to the 3D data using R1.

Discussion

3D as a reference, and a standardized method for the analysis of leaf microCT scans using free, open-source software

Our use of microCT allows for a more geometrically accurate investigation of both plant structure and function, and an in-depth investigation into how close traditional 2D estimates match the actual 3D geometry of complex surfaces within the leaf. Here, we present a standardized method for extracting leaf airspace features and for estimating S_m, an important leaf trait that is correlated with internal gas exchange and photosynthetic capacity.

Using microCT on fresh leaf samples allowed us to more fully capture the 3D mesophyll surface exposed to IAS without the potential artifacts associated with traditional light microscopy, while at the same time removing the need to correct for cell curvature and complex geometry. In this way, we could more easily measure volumetric features such as porosity of the airspace, mesophyll volume, and vein volume. Other features could be measured, such as individual cell volume and surface area by hand drawing the contour of cells. One other advantage of the microCT leaf scans is that they can be used to generate volumetric meshes for use in finite element modeling, as shown in Ho *et al.* (2016).

Limitations do exist, however, when using microCT for quantifying leaf anatomical traits. One limitation for studying leaf IAS is microCT resolution. Synchrotron microCT instruments are probably the most efficient because of the very high energy and flux of the X-rays, making a scan possible under 20 minutes or less, compared to up to 12 h on a commercial machine for a scan with a similar resolution and accuracy (Yannick Staedler, University of Vienna, personal communication). Such time savings can significantly reduce potential imaging artifacts due to tissue movement or dehydration during the scan. Magnification is also a potential limitation which typically does not exceed a voxel

resolution of ~ 0.3 μm^{-3} (the resolution available for the present study was 0.64 and 1.27 $\mu m\ pixel^{-1}$). Using light microscopy, this can be substantially lower depending on the microscope, which can show minute details that cannot be seen using microCT, although with the inherent tradeoff of decreased field of view at higher magnification, a limitation of optical microscopy systems in general. Light microscopy also has the advantage of being able to stain the sections, which allows for chloroplasts, organelles and compounds to be easily distinguished. Hence, it is difficult to accurately identify the mesophyll's distribution without prior knowledge of a leaf's anatomy and a microCT scan likely needs to be combined with a stained cross section to identify these tissues (e.g. Ho et al. 2016 had to artificially create organelles for their modelling). Finding suitable X-ray contrast agents could facilitate the extraction of specific membranes and organelles, along with improving the contrast between the airspace and the cells, as was done on flowers (Staedler *et al.*, 2013).

One key issue with the analysis of microCT data is the large file size of the mesh used to represent the surface of the mesophyll-airspace interface. This size is controlled by changing the resampling rate in BoneJ, and decreasing the resampling rate renders triangles (i.e. the mesh faces) of smaller size. Using the smallest value, 1, results in a more jagged rendering, but more accurately represents the original geometry, while increasing the resampling rate increases triangle size and hence smooths the rendered surface. Thus, it is essential to report this rate and to investigate if substantial differences between two rates exist (e.g. Figure 3). However, all inter-method analyses were done with consistent resampling rates, avoiding scale dependent differences.

Although using a smaller resampling rate leads to a more accurate representation of the airspace, a smaller mesh size requires greater memory for processing the stack. For example, using the *Particle Analyser* function of BoneJ to analyze the surface area of the *Gossypium* image stack (file size of 56 Mb) required ~1.7 Gb of RAM for R1 (30 times the file size for 17.16 x 10^6 triangles), and ~800 Mb of RAM for R2 (14 times the file size for 3.31 x 10^6 triangles; analysis ran on a 2.6 GHz Intel Core i7 laptop with 16 Gb of RAM). The average file size was between 500 and 700 Mb, and those were easy to process on the laptop mentioned above. However, some stacks had a size over 1 Gb, and to analyze

those in their entirety, we had to rely on a virtual machine (8 cores and 64 Gb of RAM), and it still led to over 50 Gb of RAM used in some cases when using R1.

Critical evaluation of methods applied to leaf sections and the validity of 2D analyses

Several methods have been presented in the literature since Turrell's (1936) to estimate S_m. Yet, as mentioned by Sack *et al.* (2013), no critical evaluation has been carried out. The increasing availability of large leaf trait databases (e.g. TRY database; www.try-db.org) and efforts to discover more general relationships among leaf traits (e.g. Onoda *et al.*, 2017) point toward a need for methodological standardization. In the introduction, we presented a list of existing methods for estimating S_m and focused on four common and contrasting methods found in the literature. The four methods evaluated produced substantially different results relative to 3D values (see Table 1 and Figure 4). Unsurprisingly, the method which assumes that the entire cellular surface is exposed to the IAS (Sack *et al.*, 2013) produces the highest values. There have been a few methods over the years which estimated the total mesophyll cell surface area per leaf area, as opposed to that which is exposed to the IAS. While most studies explicitly made this distinction (e.g. Nobel *et al.*, 1975; Longstreth *et al.*, 1985; Ivanova & P'yankov, 2002), both measurements can be found in the same reference for the same trait notation, which can generate confusion (Sack *et al.*, 2013). While the total mesophyll area per leaf area is a relevant trait to measure, it leads to substantially higher values than with the other methods that explicitly measure the mesophyll surface exposed to the IAS. Consequently, measurements using these two types of methods should not be compared together. Fortunately, a recent report made this distinction in their dataset available (Onoda *et al.*, 2017). To avoid confusion, we recommend using A_{mes}/A when the total mesophyll surface is measured, and defining S_m as the surface area exposed to the IAS, as this has been used in the most cited references (e.g. Evans *et al.* 1994).

Of the three other methods, Thain (1983) and Turrell (1936) stand out for how well they approximate 3D values, often within 10% of the 3D S_m at a R1, which we consider the standard in this study. The Turrell (1936) method produced the most accurate estimates, typically within 10% of $S_{m,3D\text{-}R1}$ (15 out of 23; 65%). However, Turrell's method necessitates a large number of sections. While it was easy to virtually slice through each

palisade layer with our 3D image stack, doing so with an embedded sample requires more expertise, especially when cutting precisely though each layer. We thus recommend this method for users who are very experienced with anatomical techniques or when a small sample size allows for more meticulous work.

The Thain (1983) method is not a measurement technique as Turrell presented, but instead applies a generic correction factor (*F*) to adjust the length of mesophyll perimeter exposed to the IAS to account for the curvature of cell walls within the section. A curvature correction could be applied to each cell, but usually only one correction factor is used for the whole leaf section. This correction factor is most usually the average of the palisade and spongy *F* values (Galmés *et al.*, 2013; Theroux-Rancourt & Gilbert, 2016). The Thain (1983) method is the most commonly used method to produce S_m estimates in the recent years. Although less $S_{m,Thain}$ estimates fell within 10% of $S_{m,3D\text{-}R1}$ compared to Turrell (13 out of 23; 57%), it requires low effort and still produces relatively reliable estimates.

We further compared our 3D estimates to the common practice of embedding leaf samples to prepare cross sections for analysis using optical microscopy. As microCT samples and the sections from embedded material often presented different leaf thicknesses, we compared the length of mesophyll exposed over the mesophyll area ratio, as suggested for CAM plants (Nelson *et al.*, 2005). This allowed us to standardize the actual exposed surface present per unit mesophyll area in the section. Using the same leaf, 2D estimates acquired from embedded material resulted in similar surface estimates to 3D estimates when the leaves were thin (~100 µm), while they diverged as leaves became thicker (~ 400 µm) (Figure 7). The more important deviations between the embedded and microCT results could be explained by in several ways. First, thick leaves tended to be CAM-type which can be more difficult to embed and section due to their weaker cell walls, thicker cuticles, and a high fiber content. This could modify leaf thickness and thus slightly compress some cells, leading to less surface being measured. There have been limited reports about the presence of distortions and shrinkage of cells following the embedding of plant leaves (Winter *et al.*, 1993; Talbot & White, 2013), and this effect might be amplified in CAM leaf samples. Hence, the tendency to underestimate thicker leaves using light microscopy might not have to do with leaf thickness but instead

493 be related to other traits associated with CAM leaves and the embedding process. Further,
494 thicker leaves might be more prone to anatomical variations between the leaf sections,
495 which, over such a volume, might lead to greater variation in the amount of exposed
496 surface. However, the differences are not caused by the user analyzing the embedded
497 slice as both lead authors independently measured values within 5% of each other using
498 two different approaches (data not shown). While adding more species to this comparison
499 would improve our confidence, we can assume that for most species the embedding
500 process would lead to S_m values in a reasonable range to microCT data, and hence
501 Thain's method is appropriate for embedded material.
502
503 *More replications needed for leaves with highly diverged veins*
504 Using our binary stacks of leaf cross sections, we showed that for ~40% of the
505 studied species, only one section was needed to produce a $S_{m,Thain}$ estimate within 10%
506 of the whole leaf median, 95% of the time (Figure 4a), and 65% of the species need three
507 slices or less. A common practice is to measure S_m over at least three slices (e.g. Evans
508 *et al.*, 1994; Tholen *et al.*, 2008; Tosens *et al.*, 2012). Hence, for a high number of species,
509 averaging S_m from at least three slices would provide estimate close to the leaf median.
510 However, several species needed to be averaged over a higher number of slices to get a
511 S_m value within 10% of the leaf median. This was not related to the raw S_m value (Figure
512 4b), but rather to the anisotropy in leaves found in certain species, which is commonly
513 associated with leaf venation patterns (e.g. Fujita & Mochizuki, 2006). Looking more
514 closely at the species differences, we found that those needing the fewest slices were
515 mainly parallel-veined leaves such as monocots, or species with weakly diverged veins
516 (e.g. *Myriopteris* and *Nymphaea*). For species possessing highly diverged veins, the
517 number of slices needed increased substantially, and up to 30 slices if the goal is to reach
518 5% of the leaf median. Fortunately, those outliers were caused by a high proportion of
519 vein in the slices (Figure 5), which were included in our method automated over the whole
520 leaf stack, and this becomes obvious by examining the relationship between the number
521 of slices and the ratio of the $S_{m,2D}$ median and standard deviation (Figure 4c). Ultimately,
522 it is up to the person doing the study to determine how many slices he or she needs. Our
523 case is an exception as we compared a minimum of 200 slices. In doing this, we identified

that removing the slices with a substantial vein fraction, a subjective filtering commonly done on microscopy slices, decreased the number of slices needed, resulting in 83% of species requiring three slices or less to be within 10% of the leaf median -- a deviation that we considered appropriate. However, one might look at 10 slices, for example, and find that variability is high, which suggests that more slices are needed.

Conclusion and recommendations for proper use and reporting of 2D methods

We describe in this paper a standardized method to reconstruct, extract, and analyze plant leaves scanned with microCT, based entirely on open-source software. For a diverse anatomical and phylogenetic set of 23 species, we compared our 3D S_m estimates with four 2D methods commonly found in the literature – treating the microCT stacks as a digital leaf sample, a most appropriate tool for this comparison. The method of Sack *et al.* (2013) produces the highest values as it estimates the entire cell surface and not just the surface exposed to the IAS. The method from Turrell (1936) is the most accurate as it often estimates 2D S_m to within 10% of the 3D value, but it necessitates the highest number of leaf sections, both cross section and paradermal. The method of Thain (1983) is the easiest to apply and produces reliable estimates, and so would be the method of choice for most researchers without access to microCT. This method also produces reasonable results when comparing with embedded leaf samples, the most common way of estimating S_m in the literature. Hence, the Thain (1983) and Turrell (1936) methods are valid and comparable among themselves, and they should be the only methods used when comparing data from different sources in the literature. Moreover, to improve the reporting and quality of S_m estimates, we recommend that at least three cross sections should be averaged when using 2D methods, with particular care when analyzing species with highly diverged veins. Regarding notation, we recommend reporting A_{mes}/A when the total mesophyll surface is measured (e.g. Nobel *et al.* 1975; Sack *et al.* 2013), and defining S_m as the surface area exposed to the IAS. Finally, when applying the Thain (1983) curvature correction method we suggest that authors measure and report values for each tissue, as opposed to using existing values in the literature.

Acknowledgments

We thank Adam Roddy for sample collection, Pat Kysar for the preparation of the embedded leaf cross sections, Ernesto Sandoval for the material collected at the Botanical Conservatory at UC Davis, and to Holly Forbes for the material collected at the UC Berkeley Botanical Garden. G.T.R. was supported by a *Katherine Esau Postdoctoral Fellowship* and a postdoctoral scholarship from the *Fonds de recherche du Québec – Nature et technologie.*

Author Contributions

GTR and JME conceived the study, developed the method and analyzed the data, with methodological inputs from MAZ, CRB, and MEG. GTR, JME, CKB, MAZ, AJM, and CRB acquired the data. GTR and JME wrote the manuscript, with contributions from all authors.

References

Bozzola JJ, Russell LD. **1999**. *Electron microscopy: principles and techniques for biologists*. Jones & Bartlett Learning.

Chabot BF, Chabot JF. **1977**. Effects of light and temperature on leaf anatomy and photosynthesis in Fragaria vesca. *Oecologia* **26**: 363–377.

Chatelet DS, Clement WL, Sack L, Donoghue MJ, Edwards EJ. **2013**. The evolution of photosynthetic anatomy in *Viburnum* (Adoxaceae). *International Journal of Plant Sciences* **174**: 1277–1291.

Davis TJ, Gao D, Gureyev TE, Stevenson AW, Wilkins SW. **1995**. Phase-contrast imaging of weakly absorbing materials using hard X-rays. *Nature* **373**: 595–598.

Doube M, Kłosowski MM, Arganda-Carreras I, Cordelières FP, Dougherty RP, Jackson JS, Schmid B, Hutchinson JR, Shefelbine SJ. **2010**. BoneJ: Free and extensible bone image analysis in ImageJ. *Bone* **47**: 1076–1079.

Dowd BA, Campbell GH, Marr RB, Nagarkar VV, Tipnis SV, Axe L, Siddons DP. **1999**. Developments in synchrotron x-ray computed microtomography at the National Synchrotron Light Source.Bonse U ed. SPIE, 224–236.

El-Sharkawy MA, Hesketh J. **1965**. Photosynthesis among species in relation to characteristics of leaf anatomy and CO_2 diffusion resistances. *Crop science* **5**: 517.

Evans JR. **2013**. Improving photosynthesis. *Plant Physiology* **162**: 1780–1793.

Evans JR, Caemmerer von S, Setchell BA, Hudson GS. **1994**. The relationship between CO_2 transfer conductance and leaf anatomy in transgenic tobacco with a reduced content of rubisco. *Australian Journal of Plant Physiology* **21**: 475–495.

Evans JR, Kaldenhoff R, Genty B, Terashima I. **2009**. Resistances along the CO_2 diffusion pathway inside leaves. *Journal of Experimental Botany* **60**: 2235–2248.

Fujita H, Mochizuki A. **2006**. The origin of the diversity of leaf venation pattern. *Developmental Dynamics* **235**: 2710–2721.

Galmés J, Ochogavía JM, Gago J, Roldán EJ, Cifre J, Conesa MÀ. **2013**. Leaf responses to drought stress in Mediterranean accessions of *Solanum lycopersicum*: anatomical adaptations in relation to gas exchange parameters. *Plant, Cell & Environment* **36**: 920–935.

Giuliani R, Koteyeva N, Voznesenskaya E, Evans MA, Cousins AB, Edwards GE. **2013**. Coordination of leaf photosynthesis, transpiration, and structural traits in rice and wild relatives (genus *Oryza*). *Plant Physiology* **162**: 1632–1651.

Gürsoy D, De Carlo F, Xiao X, Jacobsen C. **2014**. TomoPy: a framework for the analysis of synchrotron tomographic data. *Journal of synchrotron radiation* **21**: 1188–

602 1193.

603 **Ho QT, Berghuijs HNC, Watté R, Verboven P, Herremans E, Yin X, Retta MA,**
604 **Aernouts B, Saeys W, Helfen L, *et al.* 2016**. Three-dimensional microscale modelling
605 of CO_2 transport and light propagation in tomato leaves enlightens photosynthesis. *Plant,*
606 *Cell & Environment* **39**: 50–61.

607 **Ivanova LA, P'yankov VI**. **2002**. Structural adaptation of the leaf mesophyll to shading.
608 *Russian Journal of Plant Physiology* **49**: 419–431.

609 **James SA, Smith WK, Vogelmann TC**. **1999**. Ontogenetic differences in mesophyll
610 structure and chlorophyll distribution in *Eucalyptus globulus* ssp. *globulus*. *American*
611 *Journal of Botany* **86**: 198–207.

612 **Jurik TW, Chabot JF, Chabot BF**. **1982**. Effects of light and nutrients on leaf size, co_2
613 exchange, and anatomy in wild strawberry (*Fragaria virginiana*). *Plant Physiology* **70**:
614 1044–1048.

615 **Kubínová L**. **1994**. Recent stereological methods for measuring leaf anatomical
616 characteristics: estimation of the number and sizes of stomata and mesophyll cells.
617 *Journal of Experimental Botany* **45**: 119–127.

618 **Longstreth DJ, Bolaños JA, Goddard RH**. **1985**. Photosynthetic Rate and Mesophyll
619 Surface Area in Expanding Leaves of Alternanthera philoxeroides Grown at Two Light
620 Levels. *American Journal of Botany* **72**: 14.

621 **Longstreth DJ, Hartsock TL, Nobel PS**. **1980**. Mesophyll cell properties for some C3
622 and C4 species with high photosynthetic rates. *Physiologia Plantarum* **48**: 494–498.

623 **Morison JIL, Lawson T, Cornic G**. **2007**. Lateral CO_2 diffusion inside dicotyledonous
624 leaves can be substantial: quantification in different light intensities. *Plant Physiology*
625 **145**: 680–690.

626 **Morris P, Thain JF**. **1983**. Improved Methods for the Measurement of Total Cell Surface
627 Area in Leaf Mesophyll Tissue. *Journal of Experimental Botany* **34**: 95–98.

628 **Nelson EA, Sage TL, Sage RF**. **2005**. Functional leaf anatomy of plants with
629 crassulacean acid metabolism. *Functional Plant Biology* **32**: 409–419.

630 **Nobel PS**. **1976**. Photosynthetic Rates of Sun versus Shade Leaves of Hyptis emoryi
631 Torr. *Plant Physiology* **58**: 218–223.

632 **Nobel PS**. **1977**. Internal leaf area and cellular CO_2 resistance: photosynthetic
633 implications of variations with growth conditions and plant species. *Physiologia*
634 *Plantarum* **40**: 137–144.

635 **Nobel PS, Zaragoza LJ, Smith WK**. **1975**. Relation between Mesophyll Surface Area,
636 Photosynthetic Rate, and Illumination Level during Development for Leaves of

637 Plectranthus parviflorus Henckel. *Plant Physiology* **55**: 1067–1070.

638 **Onoda Y, Wright IJ, Evans JR, Hikosaka K, Kitajima K, Niinemets Ü, Poorter H,**
639 **Tosens T, Westoby M**. **2017**. Physiological and structural tradeoffs underlying the leaf
640 economics spectrum. *New Phytologist* **113**: 4098.

641 **Parkhurst DF**. **1982**. Stereological Methods for Measuring Internal Leaf Structure
642 Variables. *American Journal of Botany* **69**: 31–39.

643 **Parkhurst DF, Mott KA**. **1990**. Intercellular diffusion limits to CO_2 uptake in leaves. *Plant*
644 *Physiology* **94**: 1024–1032.

645 **Pieruschka R, Schurr U, Jensen M, Wolff WF, Jahnke S**. **2006**. Lateral diffusion of
646 CO_2 from shaded to illuminated leaf parts affects photosynthesis inside homobaric
647 leaves. *New Phytologist* **169**: 779–787.

648 **R Core Team**. R: A language and environment for statistical computing.

649 **Russin WA, Trivett CL**. **2001**. Vacuum-Microwave Combination for Processing Plant
650 Tissues for Electron Microscopy. Microwave Techniques and Protocols. Totowa, NJ:
651 Humana Press, 25–35.

652 **Sack L, Chatelet DS, Scoffoni C, PrometheuxWiki contributors**. **2013**. Estimating the
653 mesophyll surface area per leaf area from leaf cell and tissue dimensions measured
654 from transverse cross-sections. *PrometheusWiki*.

655 **Schneider CA, Rasband WS, Eliceiri KW**. **2012**. NIH Image to ImageJ: 25 years of
656 image analysis. *Nature methods* **9**: 671–675.

657 **Slaton MR, Smith WK**. **2002**. Mesophyll architecture and cell exposure to intercellular
658 air space in alpine, desert, and forest species. *International Journal of Plant Sciences*
659 **163**: 937–948.

660 **Staedler YM, Masson D, Schönenberger J**. **2013**. Plant tissues in 3D via X-ray
661 tomography: simple contrasting methods allow high resolution imaging. (M-X Sun, Ed.).
662 *PloS one* **8**: e75295.

663 **Talbot MJ, White RG**. **2013**. Methanol fixation of plant tissue for Scanning Electron
664 Microscopy improves preservation of tissue morphology and dimensions. *Plant methods*
665 **9**: 36.

666 **Thain JF**. **1983**. Curvature correction factors in the measurement of cell surface areas in
667 plant tissues. *Journal of Experimental Botany* **34**: 87–94.

668 **Theroux-Rancourt G, Gilbert ME**. **2016**. The light response of mesophyll conductance
669 is controlled by structure across leaf profiles. *Plant, Cell & Environment*.

670 **Tholen D, Zhu X-G**. **2011**. The mechanistic basis of internal conductance: a theoretical

analysis of mesophyll cell photosynthesis and CO_2 diffusion. *Plant Physiology* **156**: 90–105.

Tholen D, Boom C, Noguchi KO, Ueda S, Katase T, Terashima I. **2008**. The chloroplast avoidance response decreases internal conductance to CO_2 diffusion in Arabidopsis thaliana leaves. *Plant, Cell & Environment* **31**: 1688–1700.

Tosens T, Niinemets Ü, Vislap V, Eichelmann H, Castro Díez P. **2012**. Developmental changes in mesophyll diffusion conductance and photosynthetic capacity under different light and water availabilities in *Populus tremula*: how structure constrains function. *Plant, Cell & Environment* **35**: 839–856.

Tosens T, Nishida K, Gago J, Coopman RE, Cabrera HM, Carriquí M, Laanisto L, Morales L, Nadal M, Rojas R, *et al.* 2016. The photosynthetic capacity in 35 ferns and fern allies: mesophyll CO_2 diffusion as a key trait. *New Phytologist* **209**: 1576–1590.

Turrell FM. **1936**. The area of the internal exposed surface of dicotyledon leaves. *American Journal of Botany* **23**: 255–264.

Winter H, Robinson DG, Heldt HW. **1993**. Subcellular Volumes and Metabolite Concentrations in Barley Leaves. *Planta* **191**: 180–190.

Zhu X-G, Long SP, Ort DR. **2010**. Improving photosynthetic efficiency for greater yield. *Annual review of plant biology* **61**: 235–261.

Table 1. Anatomical data and S_m values estimated using microCT (3D) and using for 2D methods for the 23 studied species

Family	Species	t (µm)	θ_{pal}	θ_{sp}	f_{pal}	$S_{m,3D}$		$S_{m,2D}$					Thain's correction		
						R1[a]	R2	raw	JSV	Thain	Turrell	Sack et al.	F_{pal}	F_{sp}	F_{leaf}
Pteridophytes															
Aspleniaceae	*Asplenium nidus*	128		0.25	0	11.1	9.6	8.6 (1.9)[b]	8.1	12.6	10.6	25.1		1.44	1.44
Polypodiaceae	*Platycerium bifurcatum*	380	0.05	0.24	0.43	19.6	16.5	13.6 (3.5)	16.9	18.2	17.2	57.8	1.39	1.33	1.33
Pteridaceae	*Adiantum tenerum*	220	0.50	0.62	0.13	25.9	22.2	15.1 (1.3)	16.9	22.4	20.8	14.2	1.36	1.50	1.48
	Myriopteris aurea	237	0.16	0.35	0.42	28.0	23.0	19.5 (1.6)	20.8	26.7	28.9	48.7	1.52	1.27	1.38
Gnetophytes															
Welwitschiaceae	*Welwitschia mirabilis*	670[c]	0.05		1	49.5	32.9	31.4 (2.8)	48.6	47.5	45.9	157.8	1.46		1.46
Magnoliids															
Lauraceae	*Cinnamomum verum*	95	0.15	0.60	0.22	9.5	8.0	6.8 (2.0)	6.7	8.7	8.8	24.6	1.49	1.20	1.26
Basal angiosperms															
Austrobaileyaceae	*Austrobaileya scandens*	228	0.05	0.17	0.29	8.2	7.3	6.0 (1.5)	7.9	6.8	8.3	53.3	1.36	1.23	1.26
Nymphaeaceae	*Nymphaea helvola*	655	0.27	0.63	0.31	33.3	28.6	23.6 (2.4)	23.9	31.9	35.1	65.6	1.46	1.32	1.36
Schisandraceae	*Illicium floridanum*	257	0.25	0.51	0.31	13.4	12.2	9.6 (1.2)	9.8	12.2	12.0	21.0	1.42	1.21	1.28
Asterids															
Asteraceae	*Helianthus annuus*	210	0.24	0.45	0.55	24.5	19.9	17.1 (5.2)	20.1	24.0	24.8	53.1	1.51	1.31	1.42
Campanulaceae	*Brighamia insignis*	107	0.08	0.18	0.20	11.6	9.8	7.8 (1.4)	9.7	10.9	10.5	50.1	1.41	1.40	1.40
Ericaceae	*Rhododendron cilipes*	340	0.08	0.38	0.50	27.3	19.8	18.1 (2.6)	22.7	25.5	30.3	65.6	1.52	1.33	1.43
Helwingiaceae	*Helwingia chinensis*	95	0.24	0.69	0.34	12.2	11.0	8.4 (2.0)	9.0	12.2	11.1	18.2	1.45	1.38	1.40
Rosids															
Malvaceae	*Gossypium hirsutum*	304	0.20	0.36	0.57	41.6	31.9	28.8 (5.9)	30.8	41.3	37.4	75.0	1.55	1.33	1.45
Rosaceae	*Prunus dulcis*	178	0.19	0.35	0.50	31.2	21.2	18.5 (3.9)	25.7	26.4	24.3	74.7	1.49	1.43	1.46
Monocots															
Araceae	*Monstera deliciosa*	165	0.14	0.40	0.26	18.6	16.8	11.5 (1.4)	14.9	14.7	17.0	40.4	1.46	1.22	1.28
Bromeliaceae	*Aechmea fendleri*	150		0.04	0	8.2	6.8	6.4 (0.8)	7.2	8.9	8.8	35.8		1.38	1.38
	Aechmea fulgens	459	0.10	0.71	0.90	39.2	29.2	30.0 (8.6)	27.2	37.8	-[d]	69.6	1.33	1.35	1.33

	Bilbergia elegans	380	0.06	0.74	0.74	29.1	22.7	19.1 (1.5)	16.4	24.9	-[d]	51.0	1.32	1.27	1.31
	Guzmania lingulata	99	0.07	0.64	0.26	9.6	8.0	6.4 (0.6)	6.3	8.1	10.3	23.5	1.41	1.22	1.27
	Nidularium innocentii	113	0.12	0.56	0.25	12.0	10.3	8.0 (1.4)	9.5	10.5	10.4	23.0	1.35	1.28	1.30
	Puya alpestris	322	0.09	0.30	0.25	37.5	28.6	25.1 (1.9)	33.9	33.3	30.8	91.8	1.44	1.30	1.33
Orchidaceae	*Oncidium ornithorhynchum*	151		0.04	0	16.4	9.7	10.8 (1.8)	6.9	13.1	10.6	60.2		1.22	1.22

[a]: Resampling rate (R) used to produce the 3D surface: 1 = smaller grid (more detail); 2 = larger grid (smoother, but less detail).

[b]: Standard deviation in parentheses. The same sd applies to the Thain corrected values.

[c]: Leaf thickness of *Welwitschia* is 1871 µm, but the mesophyll comprises only 670 µm.

[d]: Because of the large lacunae and of the organization of the cells within the leaf profile, it was not possible to properly apply the Turrell method for those species.

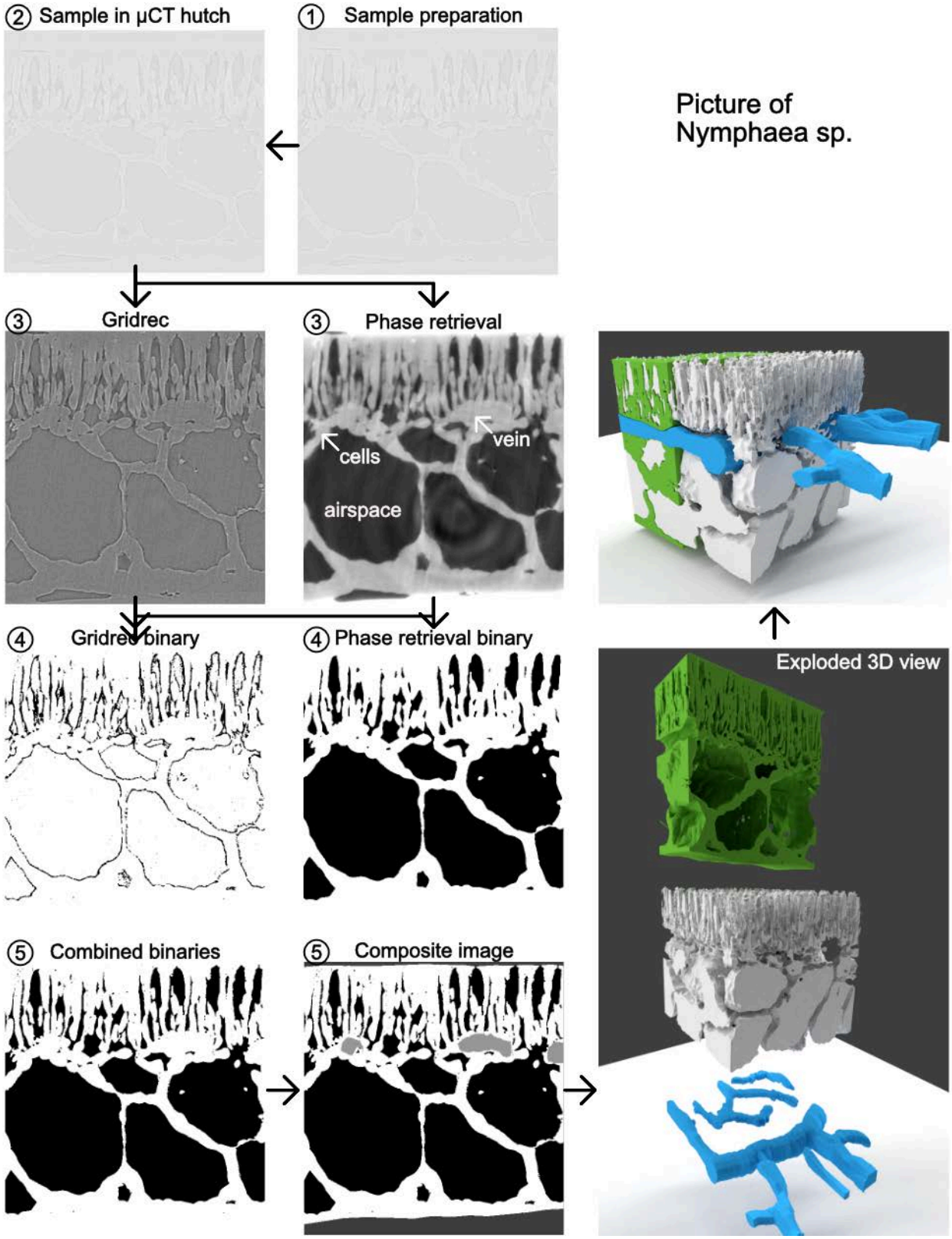

Figure 1. Graphical representation of the steps needed to produce a 3D representation of the leaf airspace, from leaf sample preparation (1) to the creation of a composite image stack with leaf airspace, cells, veins and mesophyll being segmented (5). The full description of the different steps are presented in the Methods associated with the circled numbers.

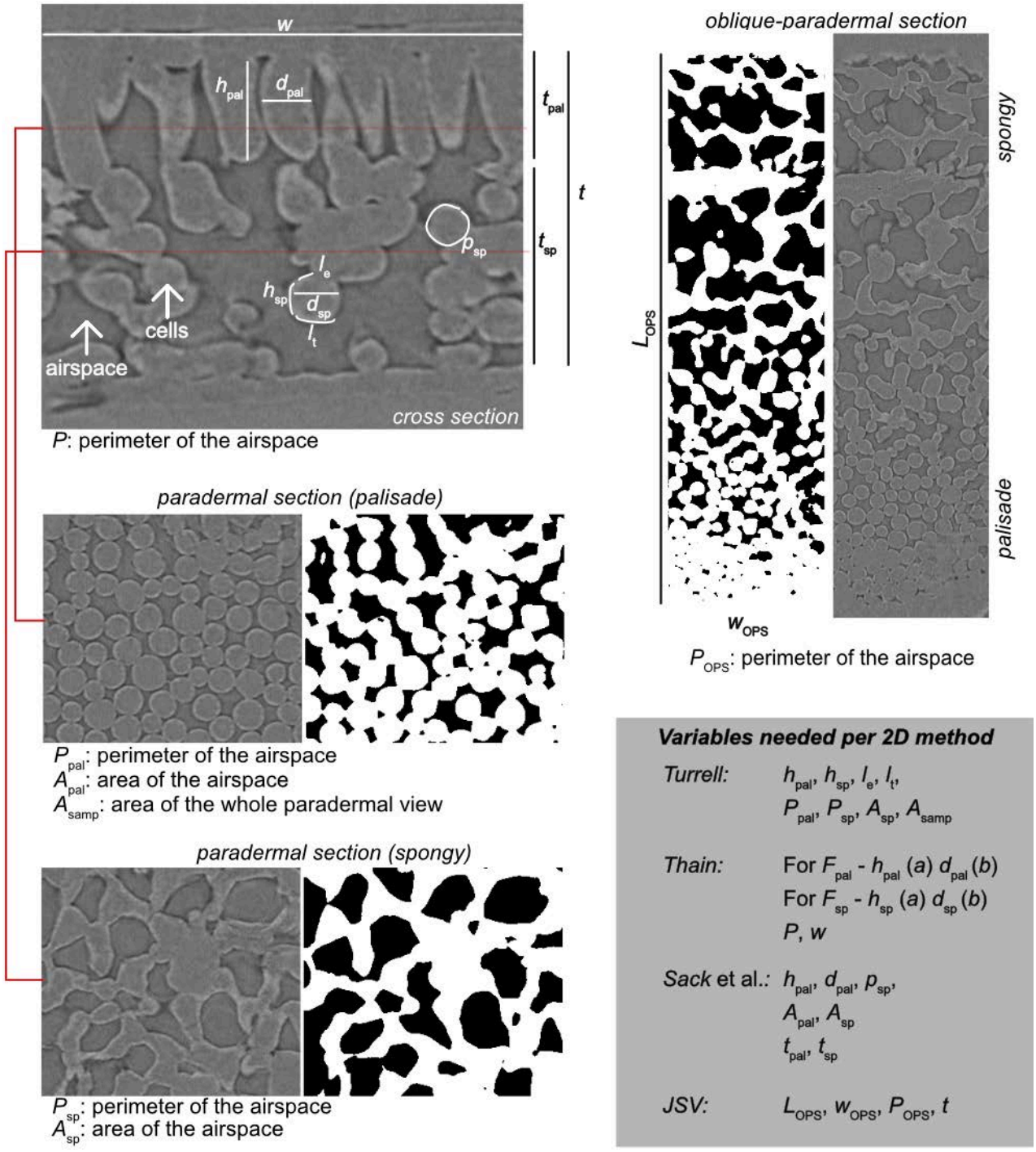

Figure 2. Graphical representation of the different variables measured on 2D sections for the four 2D methods compared in this study. For each section, the variables are drawn out when they are measured directly on cells or when corresponding to the dimensions of the section. Variables measured on binary images (airspace and non-airspace; examples presented for the paradermal and oblique-paradermal sections) are written below their respective section. A full description of each variable in presented in the Methods section. Airspace: dark or black regions; Cells: light or white regions.

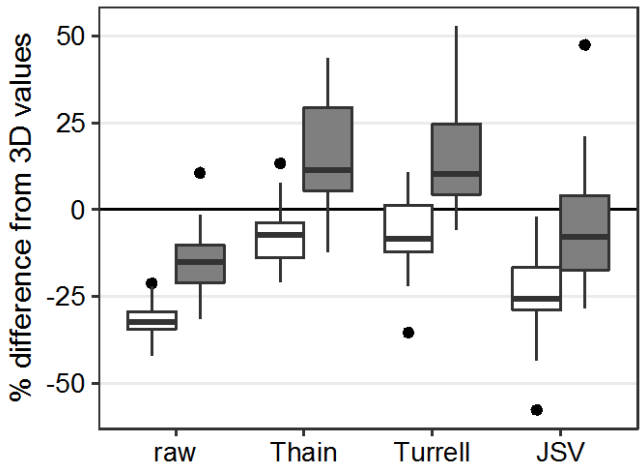

Figure 3. Error associated with different methods for estimating S_m using 2D methods compared to the microCT-derived 3D value estimated using a finer mesh size (resampling rate of 1; white boxes) and a slightly larger mesh size (resampling rate of 2; gray boxes). The raw and uncorrected 2D S_m values are presented as a comparison: it is on these values that the Thain correction was applied to. The horizontal light gray shaded area represents 10% below and above the 3D value. n = 23, except for the Turrell method where n = 21 as this method was difficult to apply for leaves with large lacunae. Estimates for the Sack *et al*. method had differences beyond the scale shown.

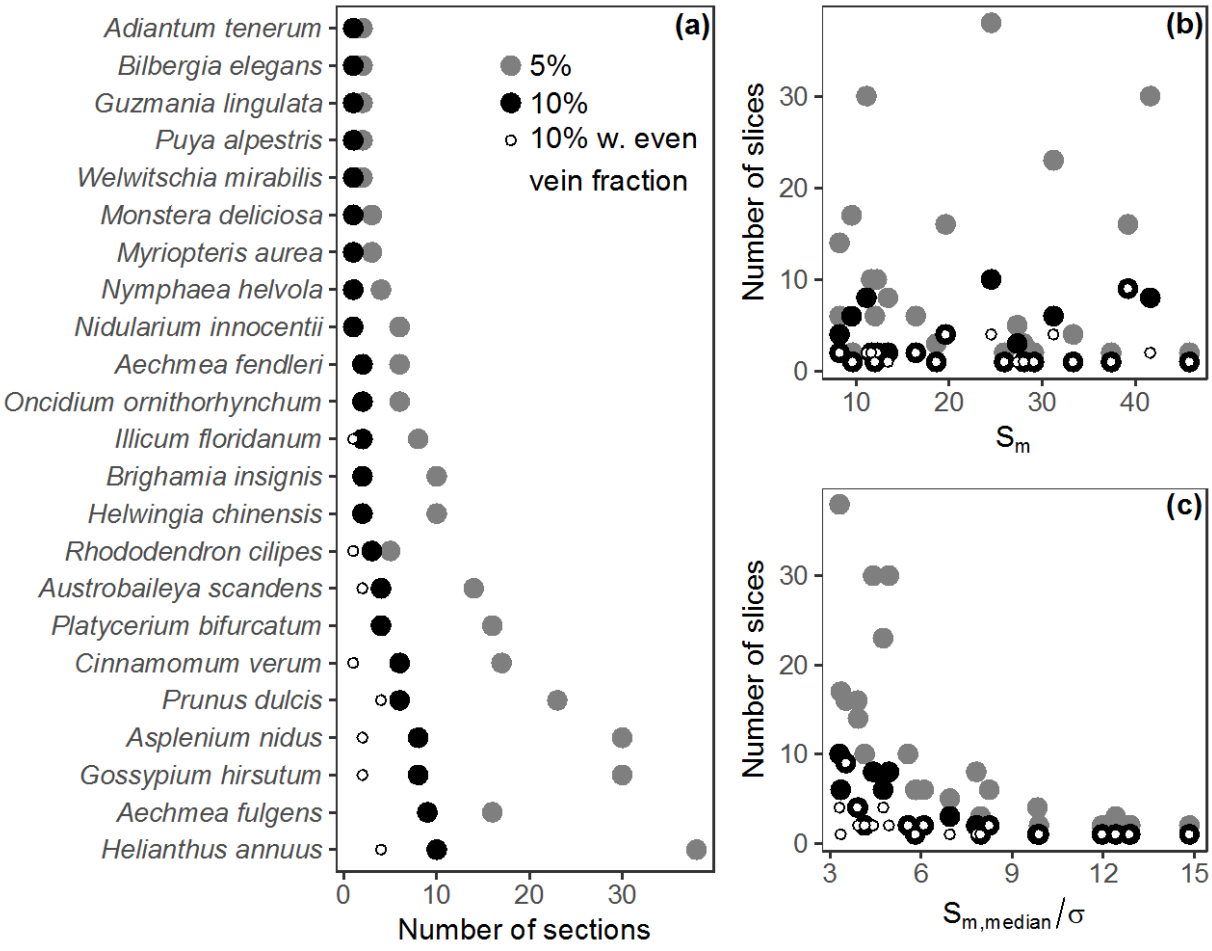

Figure 4. Number of 2D sections needed to estimate S_m within 5 (gray circles) or 10% (black circles) of the leaf level median with 95% confidence (a; left column), and the relationship between the minimum number of slices and the median S_m values (b; upper right) and with the median divided by the standard deviation (c; lower right). The minimum number of slices was also evaluated by removing the slices with too much vein coverage, a practice usually done on microscopic slices (small white circles in left plot, only when there was a different value from the black circles). This practice lead to substantially reduce the minimum number of slices needed to get within 10% of the leaf level median for most of the studied species.

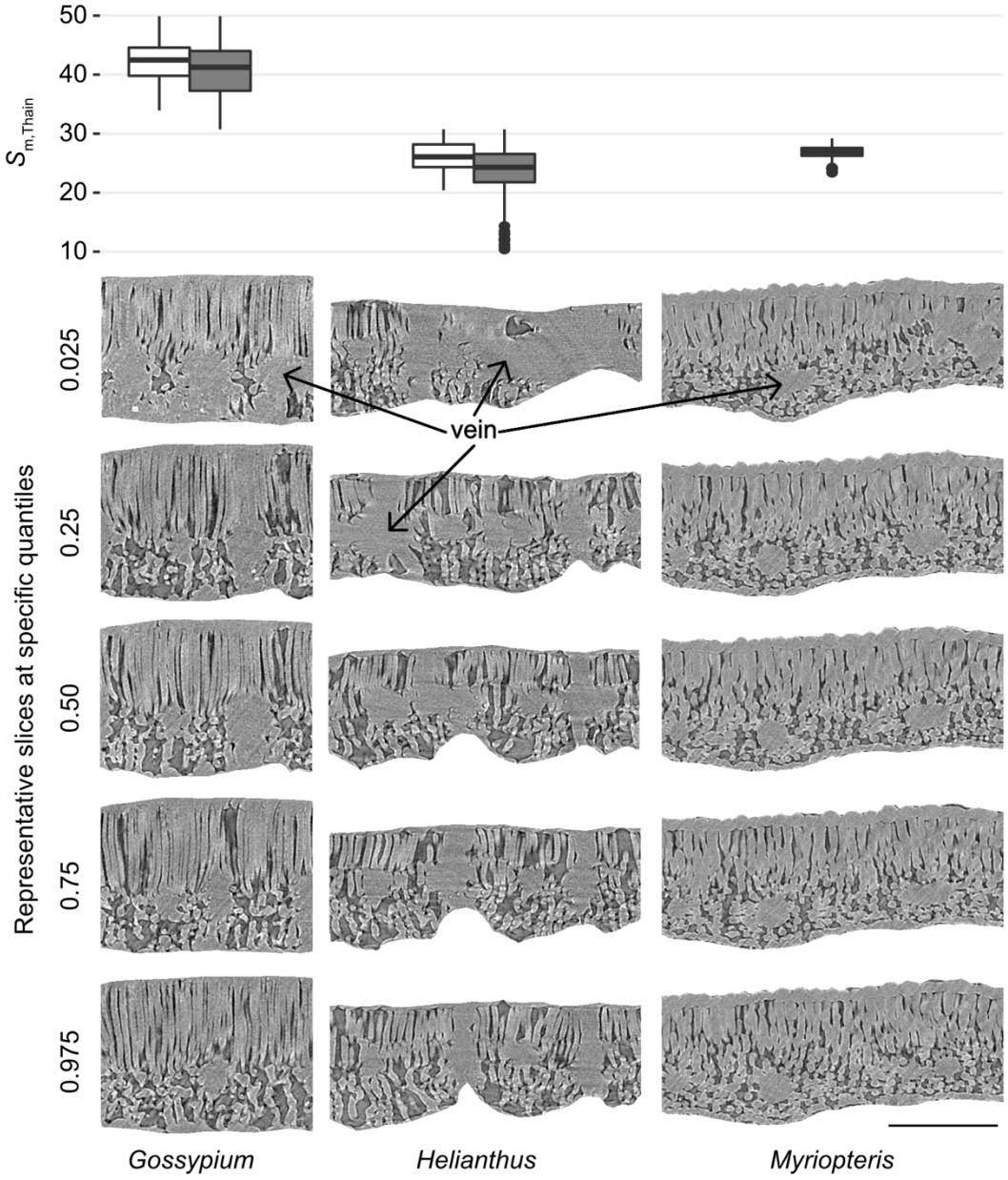

Figure 5. The effect of vein area in the calculation of S_m. Boxplot showing mean S_m values calculated from images with (gray) and without (white) slices a high fraction of vein tissue for *Gossypium*, Helianthus, and *Myriopteris*. Representative transverse microCT slices at five quantiles (0.025, 0.25,0.5,0.75,0.975) within the image stacks are shown, with veins being shown for each species.

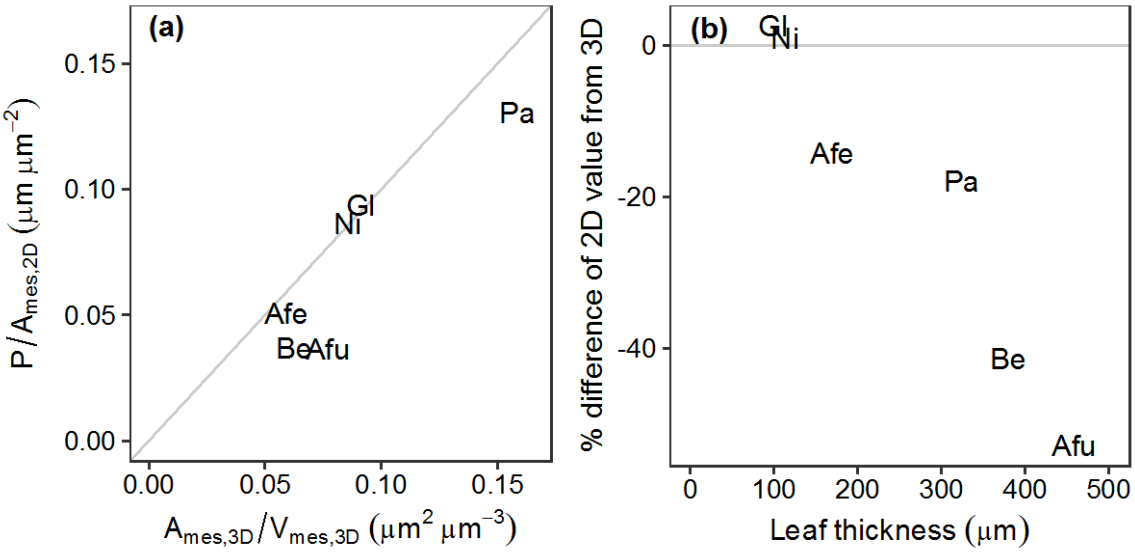

Figure 6. Deviation of 2D estimates of mesophyll surface area exposed to the IAS compared to the microCT-derived 3D value, and how the error increases with leaf thickness. (a) The relationship between the 2D-derived mesophyll perimeter exposed to the IAS (P) relative to leaf area and the 3D equivalent derived from microCT. The same leaves were used for both microCT and light microscopy analysis. (b) The relationship between the relative difference between the 2D and 3D values with leaf thickness. Species abbreviations: Afe: *Aechmea fendleri*; Afu: *Aechmea fulgens*; Be: *Bilbergia elegans*, Gl: *Guzmania lingulata*; Ni: *Nidularium innocentii*; Pa: *Puya alpestris*.

Supplementary Table S1: Growth conditions and supplementary information on the plant specimens used.

Family	Species	Auth.	Source	Growth location
Pteridophytes				
Aspleniaceae	*Asplenium nidus*		*U. of Chicago*	*Greenhouse*
Polypodiaceae	*Platycerium bifurcatum*		*U. of Chicago*	*Greenhouse*
Pteridaceae	*Adiantum tenerum*		*U. of Chicago*	*Greenhouse*
	Myriopteris aurea		*UC Berkeley Bot. Garden*	*Outdoors*
Gnetophytes				
Welwitschiaceae	*Welwitschia mirabilis*		*UC Davis Bot. Conservatory*	*Greenhouse*
Magnoliids				
Lauraceae	*Cinnamomum verum*		*U. of Chicago*	*Greenhouse*
Basal angiosperms				
Austrobaileyaceae	*Austrobaileya scandens*		*UC Berkeley Bot. Garden*	*Outdoors*
Nymphaeaceae	*Nymphaea sp.*		*UC Davis Bot. Conservatory*	*Outdoors*
Schisandraceae	*Illicium floridanum*		*UC Berkeley Bot. Garden*	*Outdoors*
Asterids				
Asteraceae	*Helianthus annuus*		*UC Davis*	*Outdoors*
Campanulaceae	*Brighamia insignis*		*U. of Chicago*	*Greenhouse*
Ericaceae	*Rhododendron cilipes*		*UC Berkeley Bot. Garden*	*Outdoors*
Helwingiaceae	*Helwingia chinensis*		*U. of Chicago*	*Greenhouse*
Rosids				
Malvaceae	*Gossypium hirsutum*		*UC Davis*	*Outdoors*
Rosaceae	*Prunus dulcis*		*UC Davis*	*Outdoors*
Monocots				
Araceae	*Monstera deliciosa*		*U. of Chicago*	*Greenhouse*
Bromeliaceae	*Aechmea fendleri*		*UC Davis Bot. Conservatory*	*Greenhouse*
	Aechmea fulgens		*UC Davis Bot. Conservatory*	*Greenhouse*
	Bilbergia elegans		*UC Davis Bot. Conservatory*	*Greenhouse*
	Guzmania lingulata		*UC Davis Bot. Conservatory*	*Greenhouse*
	Nidularium innocentii		*UC Davis Bot. Conservatory*	*Greenhouse*
	Puya alpestris		*UC Berkeley Bot. Garden*	*Outdoors*
Orchidaceae	*Oncidium ornithorhynchum*		*U. of Chicago*	*Greenhouse*

Supplementary Information

Detailed description of the four S_m methods compared in this study

1. Turrell's method: Franklin M. Turrell first reported on the surface area of mesophyll cells exposed to the IAS in 1933 (Turrell, 1933). Although he was not the first to emphasize the functional significance of the IAS, he developed a method to easily measure S_m using a camera lucida (Turrell, 1936), and this method was used in early landmark papers such as El-Sharkawy and Hesketh (1965). Turrell's method used a combination of at least two paradermal (one for each palisade and spongy layers) and one cross sections, along with simplifying geometric assumptions. For each palisade cell layer, the exposed surface was calculated as the total length of mesophyll surface exposed to the IAS in a paradermal section multiplied by the layer's height measured in a cross section. For the spongy mesophyll, Turrell assumed that the multiple cell layers had the same exposed surface area. He assumed that the entire height of the spongy cells was exposed to the IAS, but that only a fraction of the horizontal (paradermal) length was actually exposed. The exposed surface on the epidermis was also considered, as Turrell's goal was to correlate the exposed surface area to transpiration rate (e.g. Turrell, 1944), and estimate the airspace volume in the spongy mesophyll.
2. Thain's curvature correction: J. F. Thain argued in his 1983 paper that while stereological methods are likely more accurate, they are difficult when spatial heterogeneity in leaf structure exists, which commonly occurs in many species. Further, Thain warned against treating all cells as ideal shapes (e.g. spheres and cylinders) and against the averaging of single cell estimates. He recommended measuring the surfaces of all cells (as done by Dengler & MacKay, 1975), i.e. the surface exposed to the IAS. Evans et al. (1994), a much used reference for measuring and correcting S_m, also followed Thain's approach. Using this raw perimeter assumes, however, that "*all points in the section are oriented perpendicularly to the plane of the section*", which is very often invalid as the cells are curved between the two cut sides of a section. He thus presented an easy technique to correct for this unaccounted curvature of the cells. Consequently,

Thain's method is relatively low effort and is the most common found in the recent literature. To correct for the curvature of the cells, the major and minor axes are measured and averaged for a number of cells, preferably by distinguishing the different layers of cells or types of mesophyll tissue (e.g. Evans *et al.*, 1994; Galmés *et al.*, 2013; Theroux-Rancourt & Gilbert, 2016). Then, using shape specific equations, a curvature correction factor (*F*) is computed. To get a leaf-averaged *F*, the palisade and spongy mesophyll specific *F* are weighted by their respective fraction and summed (Evans *et al.*, 1994). Thain concluded his paper by saying that his method removes the "dubious" assumptions of other methods and that it should be minimally affected by the actual cell shape (e.g. see his Table 1). His method has since been validated against stereological methods, which provide similar results (Morris & Thain, 1983). Further, the Thain (1983) method requires only one cross section, but Evans et al. (1994) recommended using paradermal sections to get the true diameter of the cells.

3. JSV oblique-paradermal section method: James, Smith & Vogelmann (1999) developed a method that requires only a single section. The interest in comparing this method against the others is that it produced S_m estimates for a wide range of species (56) and families (21) (Slaton & Smith, 2002), but to our knowledge it has not been used in subsequent studies. Sectioning an embedded leaf at an angle (i.e. the cut is not at a 90° angle from the epidermis, but between 30 and 80°; see (Slaton & Smith, 2002)) produces an oblique-paradermal section (OPS). James et al. (James *et al.*, 1999) did not provide background on why this method would produce comparable or better estimates than other methods (they cite Thain (1983) and Nobel *et al.* (1975)). To compute their estimates (as simplified by Slaton & Smith, 2002) all of the exposed perimeter is measured on the section and multiplied by the mesophyll thickness to produce a surface, and ii) this surface is divided by the surface of the OPS (the width of the section along the epidermis and the length of the section from epidermis to epidermis). In other words, all the cells in the OPS are considered as one cell with a height equal to mesophyll thickness. Thus, the measured area is not simply the projected leaf area as for the two previous methods, but the actual measurement area.

4. Sack *et al.* (2013) method: Sack *et al.* (2013) present a method that allows for quantification of individual cell and tissue-level traits. This method is a re-evaluation of former methods (e.g. Nobel *et al.* 1975) that measured cell dimensions and assumed ideal cell shapes, such as spheres and cylinders. It does not measure the total perimeter of mesophyll exposed to the IAS as the former three methods. Moreover, it assumes that the entire cellular surface is exposed to the IAS. This line of methods originates mainly from Nobel *et al.* (1975). Nobel *et al.* (1975) mentioned that while the assumption of the entire cell surface being exposed to the IAS might overestimate S_m, assuming ideal shapes should compensate local irregularities in leaf cross sections leading to a reasonably accurate estimate. Sack *et al.* (2013) innovated by providing a detailed method for calculating spongy and palisade cells, the latter being divided into I- and H-shaped cells. H-shaped cells are frequent in certain *Viburnum* species, and this method was used to compare 80 species of that genus (Chatelet *et al.*, 2013). The Sack *et al.* (2013) method requires only one cross-section. Note that both Nobel *et al.* (1975) and Sack *et al.* (2013) use the notation A_{mes}/A, the surface of mesophyll over leaf area, instead of S_m, which has mainly been associated with the surface exposed to the IAS.

References

Chatelet DS, Clement WL, Sack L, Donoghue MJ, Edwards EJ. **2013**. The evolution of photosynthetic anatomy in *Viburnum* (Adoxaceae). *International Journal of Plant Sciences* **174**: 1277–1291.

Dengler NG, MacKay LB. **1975**. The leaf anatomy of beech, *Fagus grandifolia*. *Canadian Journal of Botany* **53**: 2202–2211.

El-Sharkawy MA, Hesketh J. **1965**. Photosynthesis among species in relation to characteristics of leaf anatomy and CO_2 diffusion resistances. *Crop science* **5**: 517.

Evans JR, Caemmerer von S, Setchell BA, Hudson GS. **1994**. The relationship between CO_2 transfer conductance and leaf anatomy in transgenic tobacco with a

reduced content of rubisco. *Australian Journal of Plant Physiology* **21**: 475–495.

Galmés J, Ochogavía JM, Gago J, Roldán EJ, Cifre J, Conesa MÀ. **2013**. Leaf responses to drought stress in Mediterranean accessions of *Solanum lycopersicum*: anatomical adaptations in relation to gas exchange parameters. *Plant, Cell & Environment* **36**: 920–935.

James SA, Smith WK, Vogelmann TC. **1999**. Ontogenetic differences in mesophyll structure and chlorophyll distribution in *Eucalyptus globulus* ssp. *globulus*. *American Journal of Botany* **86**: 198–207.

Morris P, Thain JF. **1983**. Improved Methods for the Measurement of Total Cell Surface Area in Leaf Mesophyll Tissue. *Journal of Experimental Botany* **34**: 95–98.

Nobel PS, Zaragoza LJ, Smith WK. **1975**. Relation between Mesophyll Surface Area, Photosynthetic Rate, and Illumination Level during Development for Leaves of Plectranthus parviflorus Henckel. *Plant Physiology* **55**: 1067–1070.

Sack L, Chatelet DS, Scoffoni C, PrometheuxWiki contributors. **2013**. Estimating the mesophyll surface area per leaf area from leaf cell and tissue dimensions measured from transverse cross-sections. *PrometheusWiki*.

Slaton MR, Smith WK. **2002**. Mesophyll architecture and cell exposure to intercellular air space in alpine, desert, and forest species. *International Journal of Plant Sciences* **163**: 937–948.

Thain JF. **1983**. Curvature correction factors in the measurement of cell surface areas in plant tissues. *Journal of Experimental Botany* **34**: 87–94.

Theroux-Rancourt G, Gilbert ME. **2016**. The light response of mesophyll conductance is controlled by structure across leaf profiles. *Plant, Cell & Environment*.

Turrell FM. **1933**. The internal exposed surface of foliage leaves. *Science* **78**: 536–537.

Turrell FM. **1936**. The area of the internal exposed surface of dicotyledon leaves.

American Journal of Botany **23**: 255–264.

Turrell FM. **1944**. Correlation between internal surface and transpiration rate in mesomorphic and xeromorphic leaves grown under artificial light. *Botanical Gazette* **105**: 413–425.